

Geomorphology of the Alluvial Sediments and Bedrock in an Intermontane Basin: Application of Variogram Modeling to Electrical Resistivity Soundings

Adnan Ahmad Khan¹ · Asam Farid² · Gulraiz Akhter³ ·
Khyzer Munir⁴ · James Small⁵ · Zulfiqar Ahmad³

Received: 3 April 2014 / Accepted: 25 January 2016 / Published online: 16 February 2016
© Springer Science+Business Media Dordrecht 2016

Abstract The study describes a methodology used to integrate legacy resistivity data with limited geological data in order to build three-dimensional models of the near sub-surface. Variogram analysis and inversion techniques more typically found in the petroleum industry are applied to a set of 1D resistivity data taken from electrical surveys conducted in the 1980s. Through careful integration with limited geological data collected from boreholes and outcrops, the resultant model can be visualized in three dimensions to depict alluvium layers as lithological and structural units within the bedrock. By tuning the variogram parameters to account for directionality, it is possible to visualize the individual lithofacies and geomorphological features in the subsurface. In this study, an electrical

✉ Asam Farid
asam.farid@gmail.com

Adnan Ahmad Khan
adnan.jadoon@gmail.com

Gulraiz Akhter
agulraiz@qau.edu.pk

Khyzer Munir
khyzer@gmail.com

James Small
jsmall@pi.ac.ae

Zulfiqar Ahmad
fz97@hotmail.com

¹ Geophysical and Data Management Technology Centre, LMK Resources Pakistan (Private), Limited, P.O. Box 44000, 9th Floor, No 55-C, PTET/Ufone Tower, Islamabad, Pakistan

² Fugro Middle East, P.O. Box 4447, Abu Dhabi, United Arab Emirates

³ Department of Earth Sciences, Quaid-i-Azam University, P.O. Box 45320, Islamabad, Pakistan

⁴ Oil and Gas Research Centre, King Abdul Aziz City for Science and Technology, P.O. Box 6086, Riyadh, Saudi Arabia

⁵ Department of Arts and Sciences, The Petroleum Institute, P.O. Box 2533, Abu Dhabi, United Arab Emirates

resistivity data set collected as part of a groundwater study in an area of the Peshawar basin in Pakistan has been re-examined. Additional lithological logs from boreholes throughout the area have been combined with local outcrop information to calibrate the data. Tectonic activity during the Himalayan orogeny has caused uplift in the area and generated significant faulting in the bedrock resulting in the formation of depressions which are identified by low resistivity values representing clays. Paleo-streams have reworked these clays which have been eroded and replaced by gravel–sand facies along paleo-channels. It is concluded that the sediments have been deposited as prograding fan-shaped bodies and lacustrine deposits with interlayered gravel–sand and clay–silt facies. The Naranji area aquifer system has thus been formed as a result of local tectonic activity with fluvial erosion and deposition and is characterized by coarse sediments with high electrical resistivities.

Keywords Naranji · Swabi · 3D kriging · Electrical resistivity sounding and paleo-channel · Geomorphology

1 Introduction

The spatial distribution of fundamental aquifer characteristics, including facies patterns and hydraulic properties, form an important factor in the study of stream processes and alluvial deposits. Well-defined empirical relationships exist between the geometric and hydraulic parameters in the development of river channels and networks, and these relationships can be applied in the interpretation of channel shapes and sizes as found in preserved strata. Previous shallow subsurface and groundwater studies have employed diverse geophysical methods to characterize a variety of aquifer types, with the main objective typically being to quantify physical properties such as lithology, fractures, porosity and permeability of the strata (Bowling et al. 2007), all of which are closely related to transmissivity and hydraulic conductivity.

Surface geophysical methods including geoelectric, geomagnetic, seismic, gravity, radioactivity, geothermometry have proven to be effective means of providing broad spatial and subsurface coverage in the detection of aquifers. During the early 1980s, the government agency of Water and Power Development Authority (WAPDA) conducted widespread geoelectrical surveys of many of the intermontane basins and valleys in the area in their search for aquifers suitable to be developed for local water supplies. Electrical resistivity techniques have long been used with considerable success as a method to infer subsurface hydrogeological conditions and geomorphological features and to detect the presence of bedrock (Stewart et al. 1983; Edmund 2009; Riddell et al. 2010; Fehdi et al. 2011; Balti et al. 2013; Mhamdi et al. 2013). Clays being relatively conductive to electric current in comparison with other coarse lithologies, therefore in fresh water aquifer systems low electrical resistivity of strata is known to be a good indication of clay content. As such, the measured electrical resistivity of alluvial deposits can be an indicator of the lithology of the subsurface conductor, although invariably the results are non-unique and of low resolution compared with well logging. The correlation between electrical resistivity of strata and physical properties of aquifers including porosity, permeability, hydraulic conductivity and transmissivity has been established in several studies (Kelly 1977; Kelly and Frohlich 1985; Mazac et al. 1988; Khalil and Santos 2013).

In this area of the northwestern Himalayan region, the evolution of many significant valley systems is primarily influenced by regional and local tectonic activity rather than from fluvial erosion or glacial attrition. Several intermontane basins have been formed as a result of uplift during orogenic episodes, and the ensuing erosion and weathering of the emergent mountain ranges generate copious amounts of sediment that is transported and ultimately deposited into valleys and topographic lows. Sedimentary processes actively work to redistribute and sort this material into talus slopes and alluvial fans and the formation of alluvial and lacustrine deposits. As a consequence, coarse-grained sediments are characteristically found deposited in the alluvial fans and stream channels which typically exhibit relatively high hydraulic conductivities. Conversely, finer-grained sediments with relatively low hydraulic conductivity accumulate in lacustrine environments. Therefore, changes in the nature of strata in terms of their lithological and geomorphological character are important factors in the development of clastic fluvial aquifers and their properties such as transmissivities and hydraulic conductivities (Bowling et al. 2005).

The original electrical surveys in and around the study area conducted by WAPDA were primarily focused on locating bedrock and regional aquifers without detailed geological interpretation. This study involved the application of variograms more often found in reservoir characterization studies in the petroleum industry. Legacy resistivity data were reinterpreted in an attempt to produce a model of the dominant fluvial systems of the project area, an intermontane basin in the northwestern Himalayan region of Pakistan. The purpose of this study was to construct a three-dimensional model of the alluvial sediments in the Naranji area in an attempt to define the primary aquifers for future groundwater development. Due to the very limited and low-resolution geophysical and geological data available from previous surveys and boreholes, it was necessary to carefully integrate all of the data before extruding the natural trends throughout the grids produced. By first establishing a rudimentary relationship between the measured resistivity and lithology in specific zones lying above and below the water table, it was then possible to propagate the resistivity field throughout the model's framework and then make the inversion to stratigraphy and implied geomorphology. Various models of the lithologies and their physical relationships were produced and evaluated for consistency. By iteratively tuning the geostatistical parameters to account for the spatial trends in three dimensions, a final model is produced which can assist in predicting zones with conditions favorable for fresh water aquifers. The techniques described can be applied on a basin-wide scale in regions where similar broad resistivity data have been previously collected and require only limited geological data from existing boreholes and outcrops for calibration.

The resultant model from the application of these stochastic modeling methods described a sedimentary system initially deposited in depressions in the form of alluvial fans and lacustrine deposits that have been reworked into gravel–sand facies forming the aquifers for the area.

2 Geology and Geomorphology of the Area

The northwest Himalayan fold and thrust belt occupies a region of approximately 250 km wide by 560 km long as an irregularly shaped mountain ranges stretching from the Afghan border up to the Kashmir basin. Intermontane basins such as the Peshawar, Haripur, Attock and Mansehra lie in this tectonic zone (Kazmi and Jan 1997). The Peshawar basin is located in the northwestern part of Pakistan as shown in Fig. 1a. The basin is bounded by

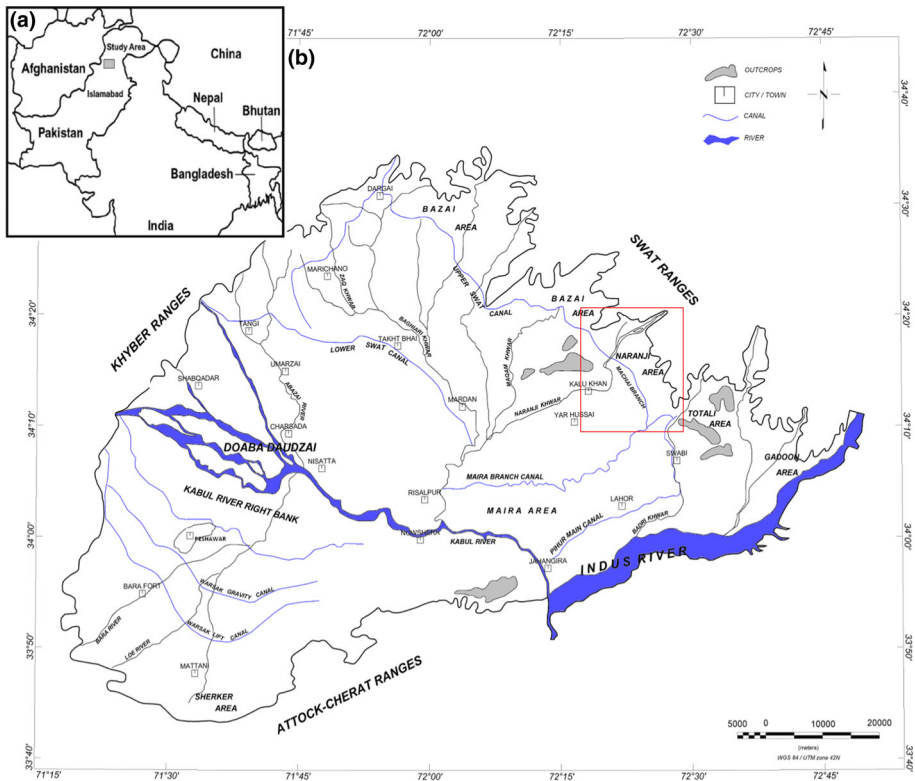


Fig. 1 **a** Regional location of the Peshawar basin (highlighted by gray box). **b** Physiography of the Peshawar basin (after Kruseman and Naqvi 1988 and Farid et al. 2013) with highlighted study area

mountain ranges including Khyber in the west and northwest, Attock–Cherat in the southwest and Swat in the northeast, while its southeastern edge is bordered by the Indus and Kabul Rivers which is open for discharge (Shah et al. 2007). The Peshawar basin has formed as a result of the Himalayan orogeny and is situated at the southern margin of the Himalayas and to the northwest of the Indus Plain (Zakir et al. 2009). The basin is situated along the junction of the northern margin of the Indo-Gangetic foredeep and the southern margin of the Hindu Kush and Himalayan ranges. The mountains in the north and northeast form a part of the Peshawar Plain alkaline igneous province. These mountain ranges are composed of granites, syenites, gneiss and schists, whereas toward the south and southwest sandstones, shales and limestones are found (Stauffer 1968; Pogue and Hussain 1986; Rafiq and Jan 1989). The Peshawar basin fill is dated to be 2.8–0.6 Ma old and comprise fanglomerates, fluvial micaceous sands and gravels (Burbank and Tahirkheli 1985). Some clay mounds are found in the area and have been formed by the shifting of the river beds and transformation of the basin into a lake during the Middle Pleistocene when outflow of the Indus was blocked (Nizami 1973; Farid et al. 2013). Figure 1b describes the physiography of the Peshawar basin with the study area highlighted in red.

The study area is about 130 km northeast of Peshawar and lies between latitudes $34^{\circ}10'–34^{\circ}21'N$ and longitudes $72^{\circ}17'–72^{\circ}30'E$. It is bounded in the north by the Ambela Range, in the northeast by Naranji Range, in the southeast by Pihur branch canal and in the

southwest by Machai branch of the upper Swat canal as shown in Fig. 2. The figure describes the physiography and geography of the study area. The Naranji area is a small part of the Peshawar basin where a structural depression has been filled with an alluvial cover of several hundreds of meters. The tectonic and sedimentary setting is identical to the Peshawar intermontane basin which was formed as a result of large-scale southward migration of Himalayan orogenic movements. Figure 3 shows the surface geology of the Peshawar basin and the adjoining areas with the study area highlighted in blue.

An alluvial fill of Quaternary age with a thickness of several hundred meters overlies the bedrock. Piedmont deposits are found near the mountains consisting of weathered bedrock. Due to frequent changes in the location of the stream beds, the lithological composition is heterogeneous both in the horizontal and vertical senses (Bloemendaal and Sadiq 1985; Akhter et al. 2012). The Naranji Khwar is the most important stream for the area and is perennial near the outlet of the area. There are many other smaller streams

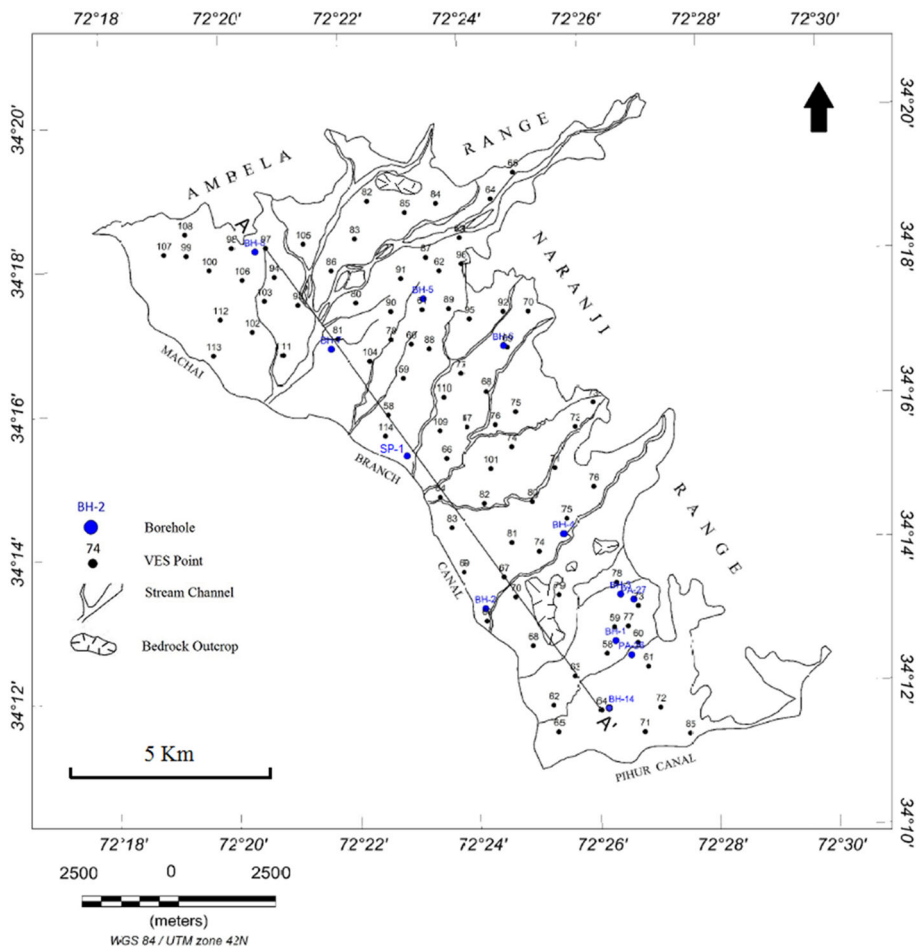


Fig. 2 Base map of the study area (after Khan and Qureshi 1990) refer to Fig. 1b

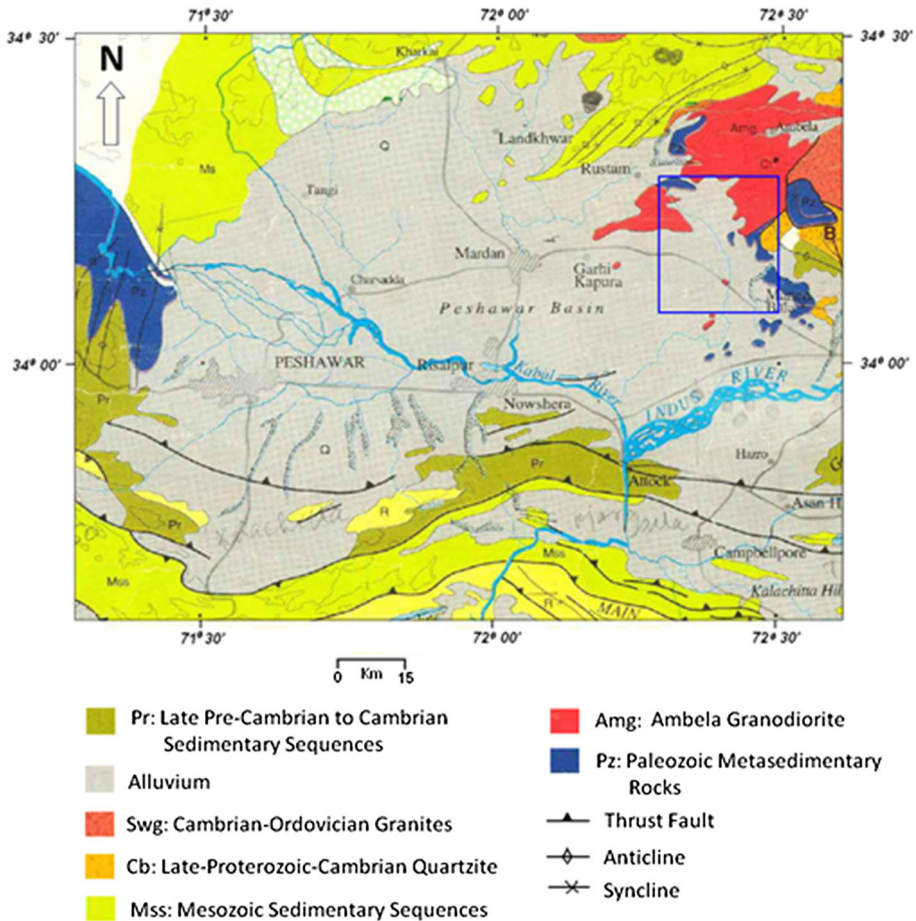


Fig. 3 Regional geology of the Peshawar basin (Searle et al. 1996; Farid et al. 2013) with highlighted location of study area

which eventually join the Kabul River. Streams are usually dry except for the lower reaches of the Naranji Khwar. In Fig. 4, boreholes (located as shown in Fig. 2) show the lithological description of the subsurface alluvial layers.

The bedrock of the catchment for Naranji Plain constitutes two main stratigraphic units, i.e., Swabi Chamla metasedimentary group and Ambela granite. The Swabi Chamla metasedimentary group comprises metamorphosed rocks of argillaceous and calcareous nature revealed in outcrops of dolomite and limestone within the plain while metamorphosed schist is evident in small outcrops in the catchment. Tectonic forces have developed fractured zones in these rocks resulting in the occurrence and movement of groundwater. Limestone also found in this group has solution cavities and underground caverns, thus forming potential reservoirs over time. The Ambela granite is an intrusive body younger than Swabi Chamla metasedimentary group which has intruded into the older rocks of the area. Ambela granite is medium to coarse grained and gradationally

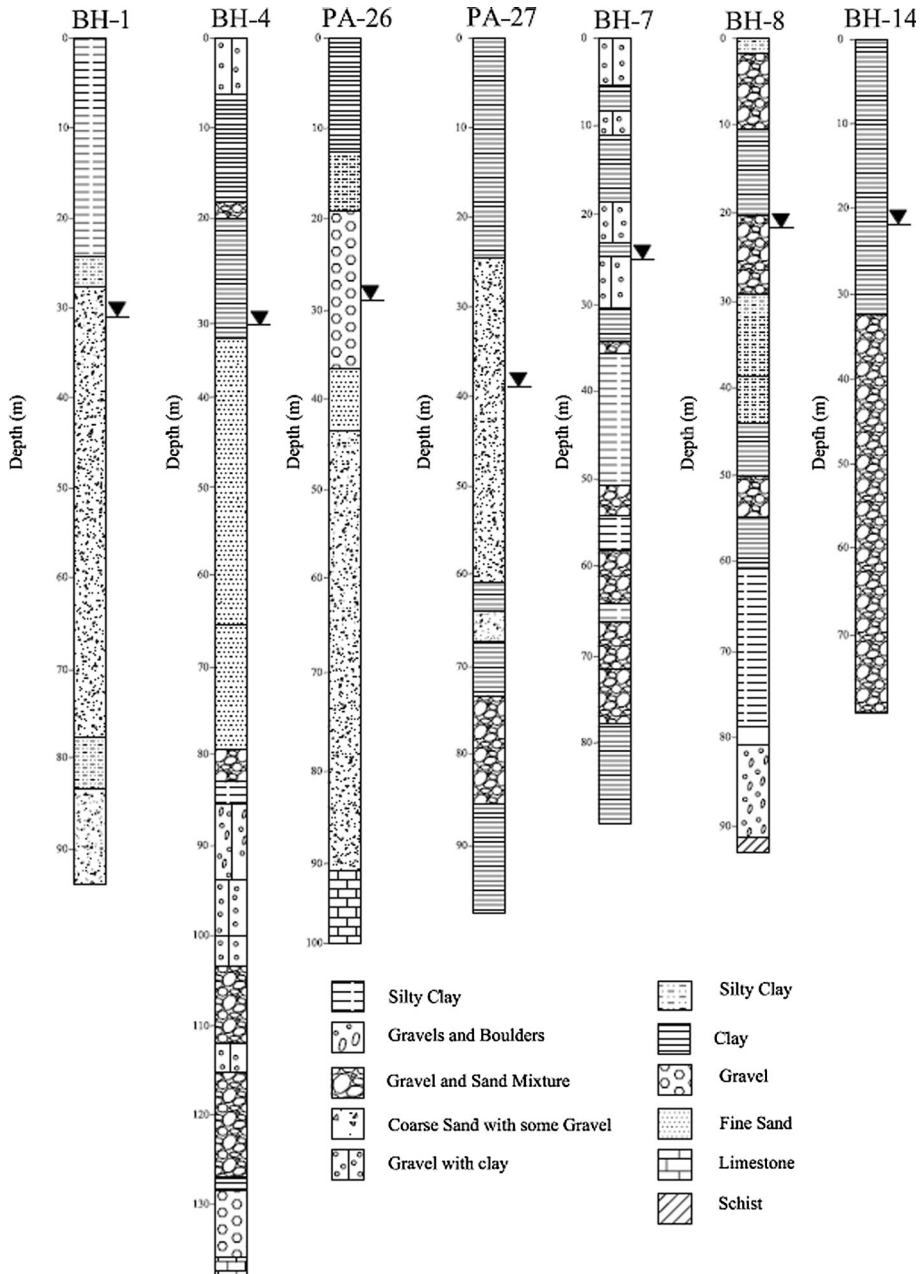


Fig. 4 Boreholes show the lithologies in the study area

metamorphosed with fracturing and joining quite common. Several springs originate in the formation which indicates the presence of groundwater in the fractured portions (Khan and Qureshi 1990).

3 Methodology

This work combines formerly measured near surface geophysical data using geostatistical methods for the visualization of paleo-geomorphic features in both two and three dimensions. Electrical resistivity data acquired as electrical sounding (ES) are processed using conventional procedures, but properties were extended using geostatistical techniques more often found in reservoir modeling. The geostatistical visualizations aid in the interpretation of the depositional setting of the study area.

3.1 Modeling and Interpretation of ES Data

The WAPDA under Pak-Dutch program acquired this ES data as a part of an investigation into the hydrogeology of the area. To cover the entire area, a total of 85 ES were collected, adopting the Schlumberger configuration with half current electrode spacing ($AB/2$) ranging from 1.5 to 500 m. For convenience, the ES were generally collected at an interval of approximately one kilometer, mostly along roads and tracks (Khan and Qureshi 1990). The directions of the resistivity measurements are variable at different locations depending upon the space available for the spread lengths. The acquisition parameters including spread lengths, overlapping points, Delta V and apparent resistivity are given in Table 1.

As is the case for many geophysical methods, interpretation of ES curves is often ambiguous where the response curve matches many different subsurface resistivity distribution models. Hence, final selection of the most appropriate subsurface model needs to be constrained by using other independent data such as surface geology and information observed from well bores. In this case, the ES data have been constrained by subsurface lithologies, water levels and distribution of electrical conductivities (EC) taken from available well bores. The data were modeled using the IPI2WIN (version 3.1.2c) software (IPIWIN-1D 2000; Zananiri 2006; Sultan et al. 2009; Farid et al. 2013) considering information derived from lithologic logs, geologic maps, subsurface water levels and EC. As an example, the measured apparent ES curve and interpreted (modeled blue curve) curves are shown in Fig. 5. The resistivity values plotted against depth are schematized into a resistivity layer model consisting of sequences of horizontal layers differentiated according to resistivity. General calibration is given in Table 2 which has been used to interpret all of the ES and to develop layer models.

Each model curve represents the simulated ES response of a horizontally stratified earth with a limited number of layers (3–6) down to certain depth and the base layer extending to infinite depth below. Each of these layers is characterized by its electrical resistivity and thickness except the base layer which does not have any thickness or has an unknown thickness. The interpreted resistivity layer models allow the subsurface electrical resistivity field to be pictured schematically to some depth. The lithology and resistivity calibration is schematized into zones delineated by water table level which ranges in depth as shown in Fig. 6 (Khan and Qureshi 1990; Bundschuh 1992). The highest resistivity ranges ($\text{Res} > 150 \Omega \text{ m}$) above the water table are associated with dry gravel–sand sediments termed as gravel–sand facies, whereas the high resistivity ranges ($\text{Res} > 150 \Omega \text{ m}$) below the water table are associated with the bedrock. The lowest resistivity ranges ($\text{Res} < 30 \Omega \text{ m}$) above and below the water table are associated with clay–silt sediments termed as clay–silt facies. The intermediate resistivity ranges (30–150 $\Omega \text{ m}$) are assigned to water saturated gravel–sand facies which constitutes the major aquifer in the area. For mapping the facies conveniently, the intermediate resistivity (30–150 $\Omega \text{ m}$) layers are

Table 1 Details of ES data acquisition parameters

MN/2 (m)	AB/2 (m)	MN (m)	AB (m)	K	Delta V	I (mA)	App. Res (Ω m)
0.3	1	0.6	2	4.76	503.95	20	120
0.3	1.5	0.6	3	11.30	265.39	20	150
0.3	2	0.6	4	20.46	161.27	20	165
0.3	2.5	0.6	5	32.24	104.23	20	168
0.5	2.5	1	5	18.84	177.28	20	167
0.5	3	1	6	27.48	122.29	20	168
0.5	4	1	8	49.46	80.88	20	200
0.5	5	1	10	77.72	52.50	20	204
1	5	2	10	37.68	109.34	20	206
1	6	2	12	54.95	72.07	20	198
1	8	2	16	98.91	35.79	20	177
1	10	2	20	155.43	21.10	20	164
2	10	4	20	75.36	42.99	20	162
2	12	4	24	109.90	26.75	20	147
2	16	4	32	197.82	13.65	20	135
2	20	4	40	310.86	5.79	20	90
2	25	4	50	487.49	3.57	20	87
5	25	10	50	188.40	9.13	20	86
5	30	10	60	274.75	6.11	20	84
5	40	10	80	494.55	3.24	20	80
5	50	10	100	777.15	1.83	20	71
10	50	20	100	376.80	3.93	20	74
10	60	20	120	549.50	2.47	20	68
10	70	20	140	753.60	1.73	20	65
10	80	20	160	989.10	1.23	20	61
10	100	20	200	1554.30	0.63	20	49
20	100	40	200	753.60	1.38	20	52
20	120	40	240	1099.00	0.73	20	40
20	140	40	280	1507.20	0.48	20	36
20	160	40	320	1978.20	0.31	20	31
20	180	40	360	2512.00	0.23	20	29
20	200	40	400	3108.60	0.17	20	27
40	200	80	400	1507.20	0.38	20	29
40	250	80	500	2390.33	0.23	20	27
40	300	80	600	3469.70	0.16	20	27
40	350	80	700	4745.33	0.12	20	28
40	400	80	800	6217.20	0.09	20	29

Delta V (mV) is the potential difference between MN; K is the geometric factor with units m

interpreted as single gravel–sand layers, thus resulting in a uniform interpreted three-layer model. For convenience, many shallow thin layers are combined into a single layer after calibration using the scheme in Table 2.

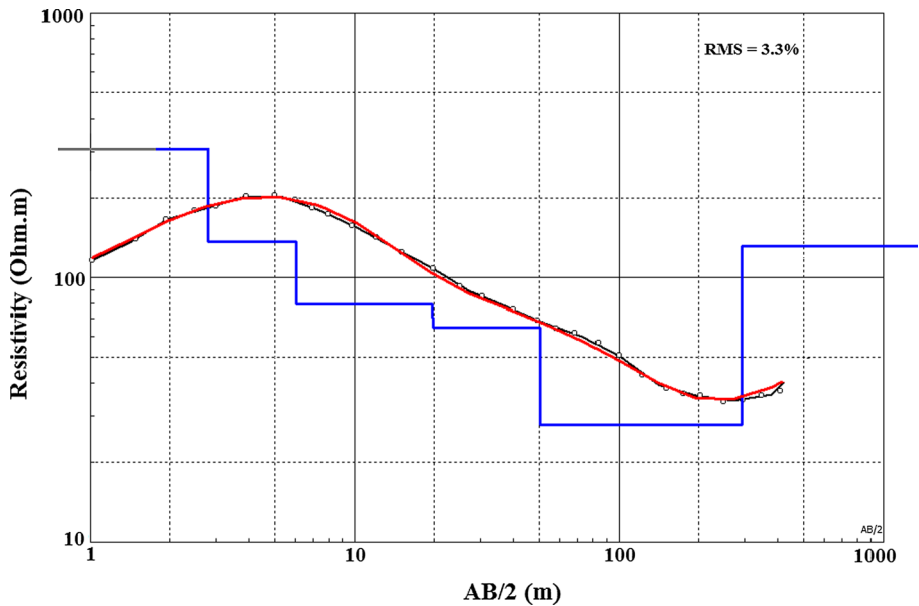


Fig. 5 Modeled electrical resistivity data for the VES number 81. *Small black circles* represent the sampled resistivity at a particular depth, the *black line* represents the line of best fit for the apparent resistivity measurements, and *blue line* represents the modeled true resistivity. The x-axis is the electrode spacing ($AB/2$) for the apparent resistivity and depth (m) for the modeled resistivity

Table 2 Calibration between different lithologies and resistivity

Formation resistivity (Ω m)	Lithology	Remarks
Res < 30	Clay–silt	Above water table
Res > 150	Gravel–sand	Above water table
30 > Res < 150	Gravel–sand	Below water table
Res < 30	Clay–silt	Below water table
Res > 150	Bedrock	Below water table

3.2 Variogram and 3D Gridding

A variogram is an important geostatistical tool for measuring the spatial variability of sampled data which can be used for interpolation and gridding purposes. The derived value of ‘variability’ increases as the input samples become more disparate. Most basic and popular gridding algorithms such as ‘least squares’ and ‘minimum curvature’ are insensitive to trends in the data and lack the ability to be ‘tuned’ to fit individual data sets. Variogram gridding and interpolation techniques require an analytical model as input in order to produce surfaces capable of reflecting the geometry and continuity of the studied phenomenon. Hence, the resultant output incorporates a level of understanding of the spatial trends inherent in the data, which forms an important aid during the interpretation process (Armstrong 1984; Cressie 1993; Olea 1995; Goovaerts 1997; Gringarten and Deutsch 2001). Thus, the geostatistical variogram has become an essential technique for correlating and quantifying the spatial relationships found in discretely sampled data.

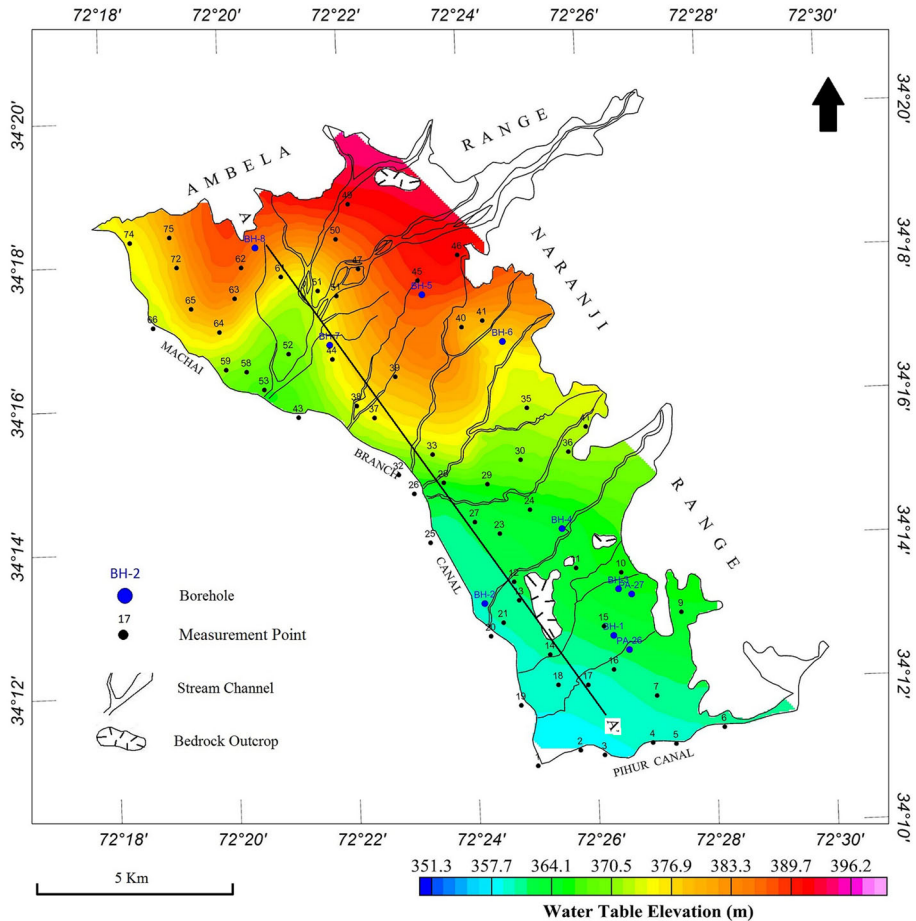


Fig. 6 Water table map which varies in depth being shallow toward the middle of the study area and deeper near the mountains

The variogram (or the semi-variogram in the simplified case) is calculated using the following expression,

$$\gamma(h) = 0.5 * E[Z(X + h) - Z(X)]^2 \tag{1}$$

where ‘ $\gamma(h)$ ’ is the semi-variance, ‘ E ’ is the expectation, ‘ X ’ is the location, ‘ h ’ is the sampling distance and ‘ Z ’ is the observed data value. The above expression provides a measure of correlation between the sampled values and their range of scatter.

As the distance between samples approaches zero (i.e., $h \rightarrow 0$), the value of the variogram should also approach zero. However, should the variogram be greater than zero in this situation, then any residual value is defined as the ‘Nugget Effect’ (C_0). The total sill (S) of the variogram is then calculated as, $C + C_0$. Often C is also known as S of the variogram model fitted to the experimental variograms when C_0 is zero.

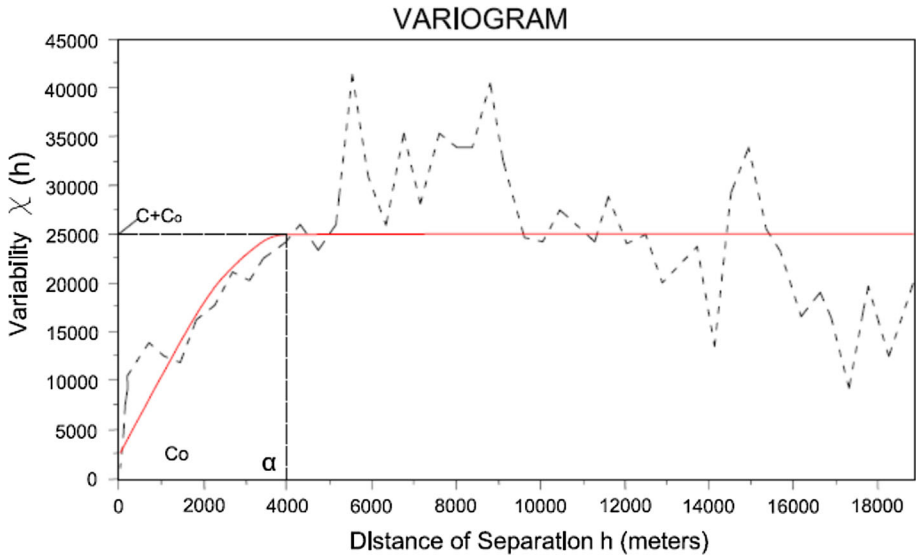


Fig. 7 Variogram for the Naranji data set. *Black line* is the experimental variogram, whereas the *red line* is the fitted model variogram

There are many possible variogram model types which can be applied in the analysis; these include linear, exponential and spherical models. Any of these basic model types will deliver adequate results for most data sets, and the spherical model was selected for this study.

The spherical model is given as:

$$\gamma(h) = C_0 + (C - C_0)[(1.5 h)/(\alpha - 0.5(h/\alpha))] \tag{2}$$

where α is the range of the variogram. The variogram in Fig. 7 shows the anticipated increase in variability $\gamma(h)$ as h increases. While the variability appears to decrease for $h > 10,000$ m, this effect is attributed to having too few data points for valid statistics.

In order to intelligently predict values between sample points, most gridding techniques will take some form of weighted averaging approach to interpolating values at grid nodes, in this a case linear weighted average is used, i.e.,

$$T = w_1g_1 + w_2g_2 + w_3g_3 + \dots + w_mg_m \tag{3}$$

where T is the estimator, $w_1, w_2, w_3, \dots, w_m$ are the weighting factors and $g_1, g_2, g_3, \dots, g_m$ are the known values at known locations, i.e., resistivity values at ES locations in this case. The weighting factors were calculated using the kriging method. Kriging is an interpolation technique based on estimating the property of an unknown location based on the spatial variability of samples. Thus, it requires the use of a model of the variogram in order to determine the weighting factors to be used in the kriging matrix defined as

$$\begin{pmatrix} \gamma_{(1,1)} & \cdots & \gamma_{(1,N)} & \lambda \\ \cdot & \cdots & \cdot & \lambda \\ \cdot & \cdots & \cdot & \lambda \\ \cdot & \cdots & \cdot & \lambda \\ \gamma_{(1,N)} & \cdots & \gamma_{(N,N)} & \lambda \\ 1 & \cdots & 1 & 0 \end{pmatrix} \begin{pmatrix} w_1 \\ \cdot \\ \cdot \\ \cdot \\ w_N \\ 1 \end{pmatrix} = \begin{pmatrix} \gamma_{(1,X)} \\ \cdot \\ \cdot \\ \cdot \\ \gamma_{(N,X)} \\ 1 \end{pmatrix} \quad (4)$$

where γ is the spherical variogram model, λ is a Lagrange multiplier used to ensure that the sum of weights is equal to one ($\sum w_i = 1$) to have an unbiased estimator, N is the number of samples and X is the unknown location where we would like to estimate the property.

All the resistivity data have been combined into a single data set without consideration for local anisotropy and orientation of ES. Geosoft Oasis Montaj (Geosoft 2013) has been used for gridding the data in 3D by using the kriging method. For the variogram shown in Fig. 7, the S parameter has been set to 25,000, α to 4000 and C_0 to 2500. The value for the C_0 is required when the smoothed line of best fit for the experimental variogram does not pass through the origin, i.e., at $h = 0$.

The software uses the statistical gridding methods using the parameters set as given in Table 3 to determine a value of resistivity at each grid cell node in three dimensions. Table 3 provides the parameters used in the 3D gridding process with resistivity values modeled to the nodes of adjacent $80 \times 80 \times 80$ m voxels. In calculating resistivity field values for the individual nodes of each voxel, the software scans for observed data values out to the maximum radius (1600 m). If more data points are found within the search radius than specified by the Maximum Points parameter, only the nearest values are used.

4 Results and Discussion

Two resistivity maps are shown as examples in Figs. 8 and 9; one map represents resistivities above the water table (at 5 m in Fig. 8) and the other map shows resistivities below the water table (at 100 m in Fig. 9). The resistivity map for 5 m depth in Fig. 8 shows two distinct geomorphic features. An alluvial fan is seen toward the north of the study area and is characterized by red–pink colors (Res > 150 Ω m as dry gravel–sand). The blue colors (Res < 30 Ω m) represent the areas where clay has accumulated in depressions. Also the

Table 3 Parameters used for 3D gridding

3D Gridding parameters	Value
Cell size	80 m
Cell size for Z	80 m
Blank distance	$12 = 12 \times 80 = 960$ m
Maximum radius	$20 = 20 \times 80 = 1600$ m
Minimum points	1
Maximum points	8
Strike	0°
Dip	90°
Plunge	0°
Strike weight	1
Dip weight	1

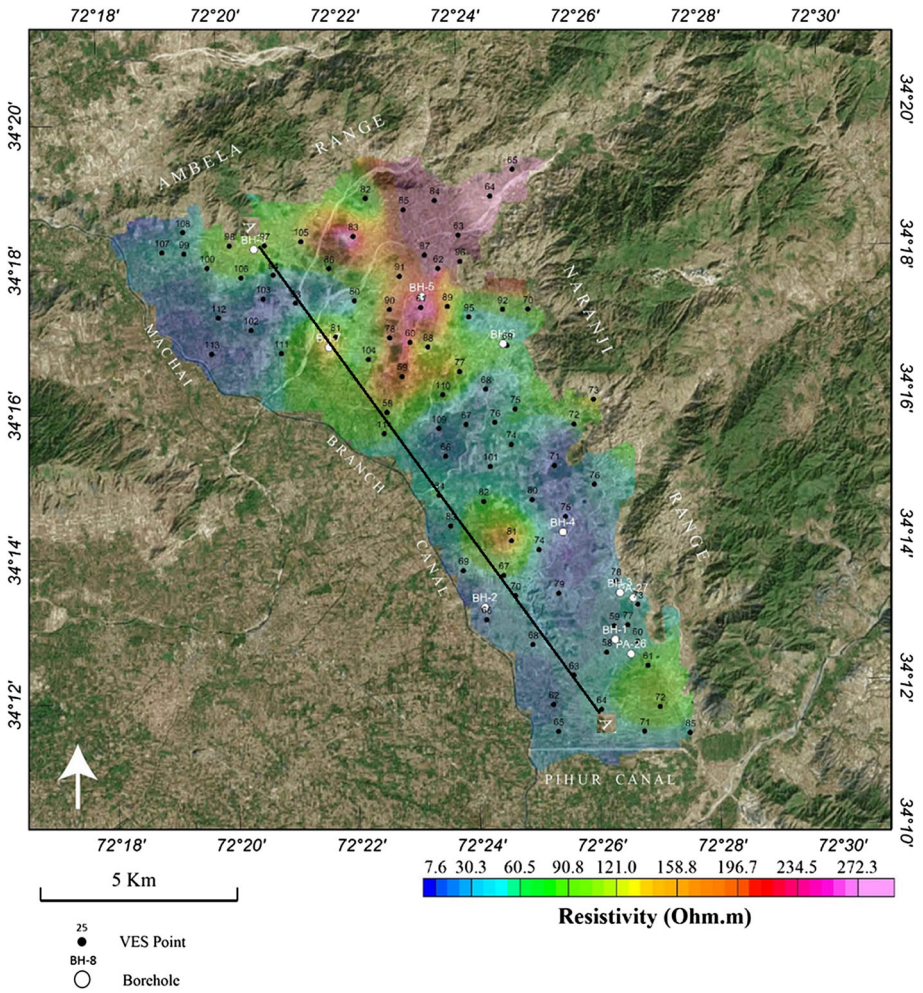


Fig. 8 Resistivity map at 5 m depth (i.e., above the water table). Two geomorphic features are evident on this map; high resistivity zone (red–pink) has been interpreted as an alluvial fan, and the low resistivity zones (blue–green) of the survey area are interpreted as clay-filled depressions. Zones of intermediate resistivity are interpreted as gravel–sand accumulation areas, which are possible targets for groundwater development. The satellite image is copyright by Google

zones of green to red colors (30–150 Ω m) represent the places of gravel–sand accumulation which are water saturated. Figure 9 shows two geomorphic features. The blue color (Res < 30 Ω m) represents the depressions where clay has accumulated. The red–pink colors (Res > 150 Ω m) represent the bedrock which outcrop in the study area. Light blue to red colors (30–150 Ω m) represent the places of gravel–sand accumulation. The major difference between the two maps, apart from one being above the water table and one being below, is the location of the presence of clays. This is interpreted as being the result of stream erosion and deposition following local tectonic activity. Figure 9 shows that the clay has accumulated in the depression generated by the tectonic activity in a standing water body such as a lake. The resistivity pattern shows that the coarse sediments such as gravel and sand are deposited near the mountains which progressively grades to fine

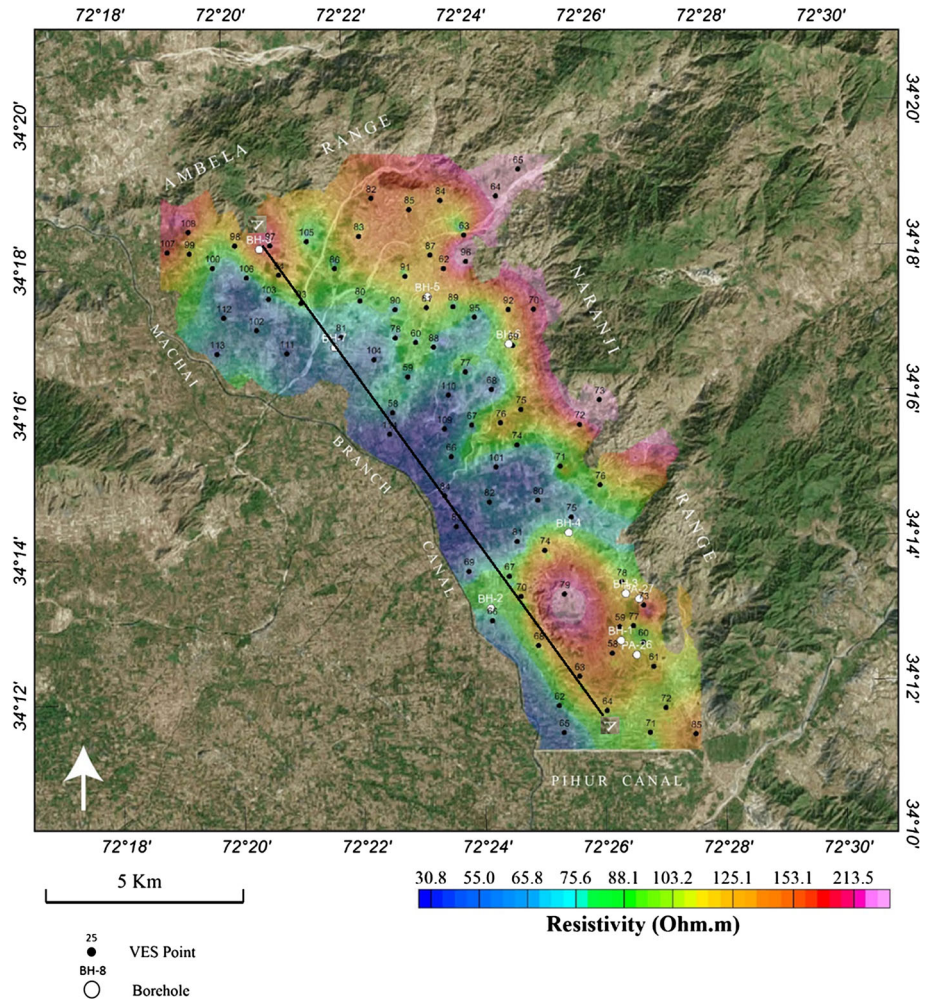


Fig. 9 Resistivity map at 100 m depth (i.e., below the water table) obtained by variogram aided 3D gridding. Two geomorphic features are evident on this map. The low resistivities are interpreted as clay-filled depressions. The high resistivities represent the bedrock. Zones of intermediate resistivity are interpreted as gravel–sand accumulation areas, which are possible targets for groundwater development. The satellite image is copyright by Google

sediments such as clay and silt toward the basin. The bedrock is composed of metasedimentary rock as evident from boreholes BH-4 and BH-8. The high resistivity ($\text{Res} > 150 \Omega \text{ m}$) closure in the southern part of Fig. 9 suggests that the uplift of the bedrock into alluvial layers either by intrusions (as evidenced by the granite outcrops in the north and northeast) or by faults took place as a result of tectonic activity.

A resistivity cross section is made from the interpolation of resistivity data along the profile AA', with the interpreted results shown in Fig. 10a, b, respectively, as a generalized two- to three-layer case. The profile suggests that the bedrock has been uplifted during the Himalayan orogeny resulting in faults being induced into the bedrock. Depressions were formed creating space for sediments derived from the adjacent mountain ranges. An

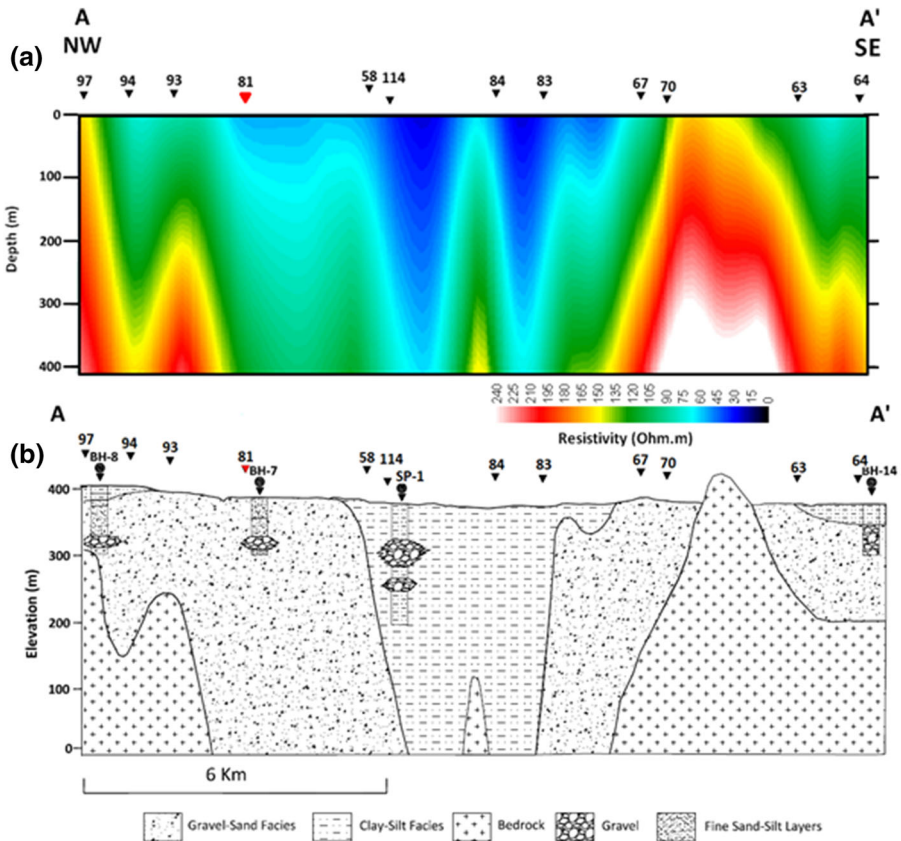


Fig. 10 Cross-sectional AA' shows the three-layer case of the subsurface. The bedrock, the clay–silt and gravel–sand facies; the presence of gravel in the boreholes SP-1, BH-7 and BH-8 confirms the braided channel erosion and deposition that took place while clay–silt facies were being deposited

example of such a depression is shown in Fig. 10a between resistivity points 58 and 83 characterized by low resistivity values. The high resistivity spike (represented by green and yellow colors) between resistivity points 114 and 84 is the result of interpolation. Figure 10b shows that the alluvial cover is quite thick toward the center of the study area along the Machai Branch canal and becomes relatively shallow toward the northern and southern boundaries. The thickness of alluvium is variable and mostly composed of sand, gravel and clay layers. A predominance of clay in the center of the profile AA' implies that at the time of deposition several large standing water bodies such as lakes were present. Similar clay deposits can be found throughout the Peshawar basin. The clay–silt facies was significantly eroded and replaced with gravel–sand deposits by various stream channels. Boreholes BH-8 and SP-1 confirm the presence of gravel patches intermixed with sand and silt within this clay–silt entity as shown in Fig. 10b. This can be attributed to the stream channels which have reworked the deposited material over time.

The underlying rocks are mostly composed of schists, limestone and quartzite of Swabi Chamla metasedimentary group, whereas Ambela granite occupies the major part of the catchment of Naranji Khwar and other smaller streams. The Ambela granite has imparted

much influence on the nature and composition of the alluvial deposits. The coarser materials are generally found near the mountain ranges, and the finer are deposited downstream. Two lithofacies can be differentiated in the plain, and their lateral and vertical extents are identified. These include gravel–sand facies and clay–silt facies. The gravel–sand facies entity is composed of fairly well-sorted thick, medium to coarse-grained sand and gravel with occasional pebbles intermixed. The lateral extent of the facies is terminated by limestone outcrops in the west and by granite in the north. These deposits make good aquifers and show a fan nature in lithology. Clay–silt facies occupies a large part of the subsurface in the plain and is characterized by hard and impervious silt and clay layers with varying thickness.

The maps show the spatial extent of the geomorphic features, whereas the cross sections show their variations in a vertical plane. The maps affirm that local depressions changed with geologic time as the sedimentation progressed and this can be confirmed from the boreholes data which show multilayers of the gravel–sand facies in the

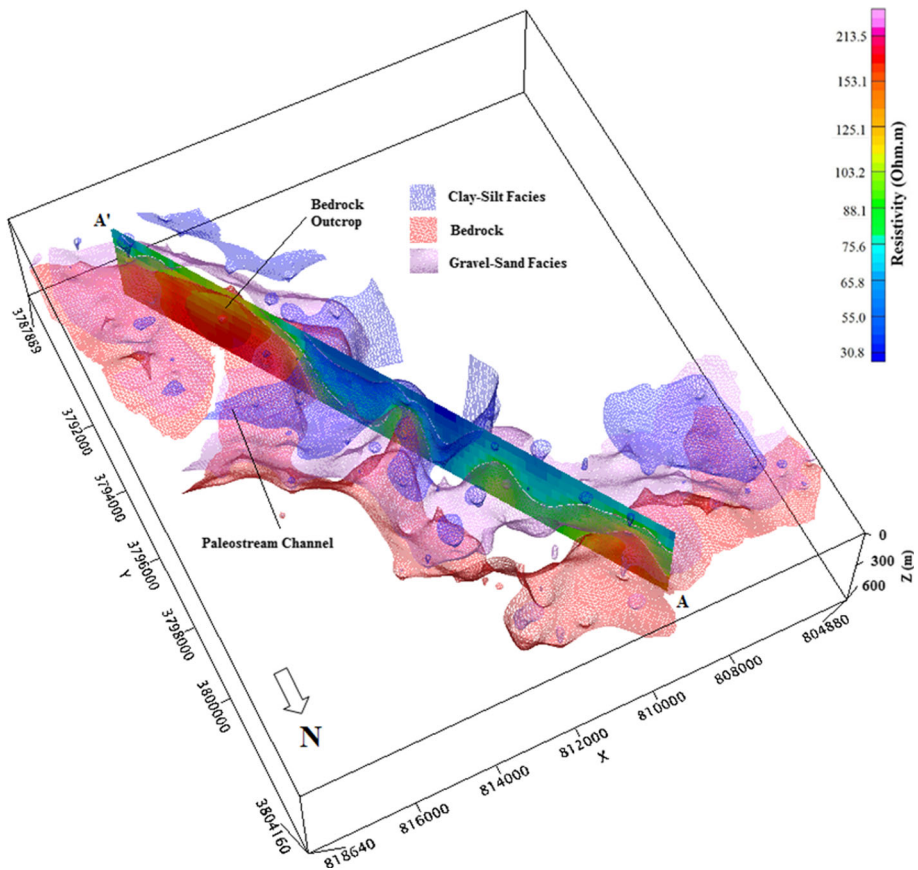


Fig. 11 Distribution of facies in the study area obtained by variogram aided 3D gridding in a 3D view. The blue color represents the clay–silt facies. The sediments prograde into the center of the study area. From the figure, it can be observed that the sediments were supplied to the basin by various paleo-stream channels. The X, Y and Z coordinates are all in meters

clay–silt facies. Figure 11 shows a 3D view of the combined facies distribution diagram in the depth domain. The locations of various facies are shown with respect to the bedrock. The blue-colored zone represents the clay–silt facies, the purple color is the gravel–sand facies and red is the bedrock. The figure confirms that sediments prograde to the center of the study area. It is observed from the figure that the sediments are supplied for the basin fill by various paleo-stream channels. The sediments are coarse near the edges (mountain ranges) characterized by gravel–sand facies and become finer toward the center of the study area.

Bedrock is found at variable depths by modeling the resistivity data throughout the area as shown in Figs. 10, 11, 12 and 13. Figure 12 shows the view from the north and Fig. 13 the view from the south. The 3D views are in agreement with the bedrock outcrop patterns as shown in Fig. 13. The bedrock outcrops in the southern part of the study area and slopes down into the basin. Both figures show the presence of paleo-stream channels cutting through the bedrock. These stream channels represent big faults in the bedrock. The bulge in the modeled bedrock further south of this stream channel is due to tectonic activity rather than an intrusion which have pushed the bedrock into the alluvial sediments.

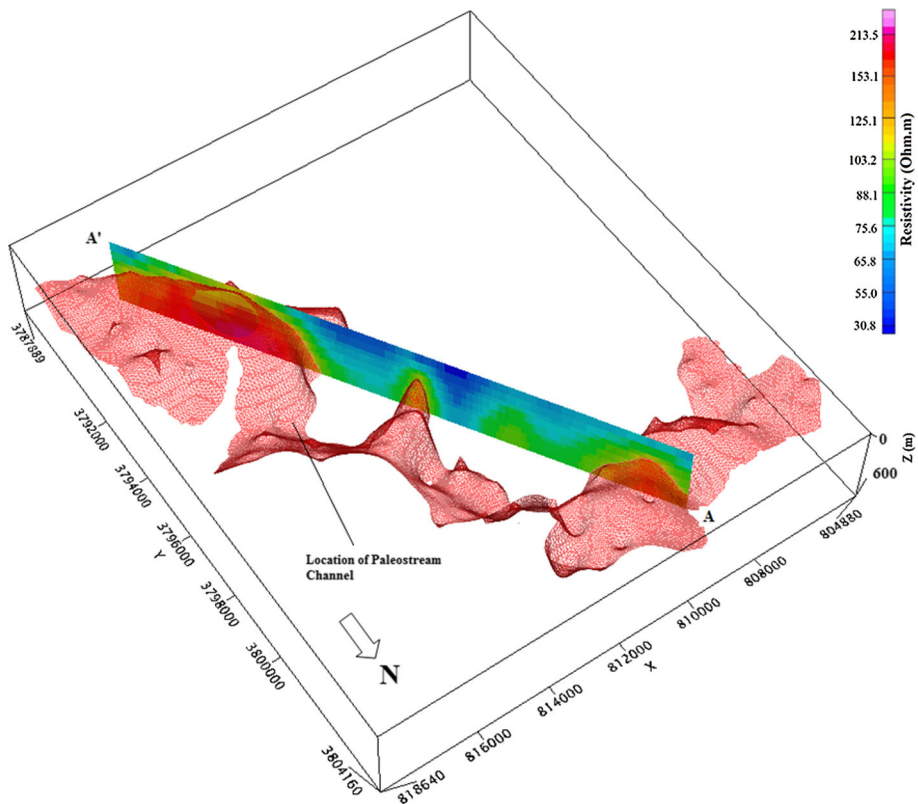


Fig. 12 Northward view of the modeled bedrock. The bedrock slopes down into the basin and also outcrops in the southwest. The presence of paleo-stream channels cutting through the bedrock can be seen where faults have been interpreted in the bedrock. X, Y and Z coordinates are all in meters

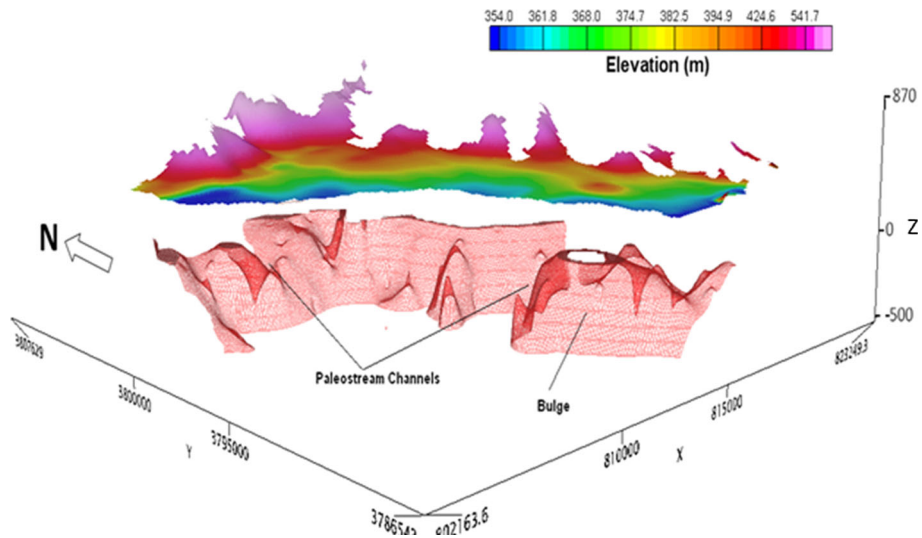


Fig. 13 Southward view of the modeled bedrock. The presence of paleo-stream channels cutting through the bedrock can be seen which represent faults in the bedrock. The surface elevation grid shows the relationship of the bedrock with the surface topography. X , Y and Z coordinates are all in meters

5 Conclusions

For the area under study, careful tuning of the variogram and gridding parameters has made it possible to identify individual lithologies and geomorphological features such as alluvial fans and depressions. Coarse sediments are recognized closer to the mountains, and these can be seen to become finer toward the center of the basin. Two lithofacies were differentiated in the plain and their lateral and vertical extents identified and mapped. In the center of the study area, the subsurface could be characterized by alternating bands of impervious silt and clay layers of variable thickness, jointly called clay–silt facies. These lithologies can be attributed to the standing water bodies in which they were originally deposited. The subsurface along the mountain ranges comprises gravel–sand facies consisting of layers of gravels, pebbles and sand intercalated with clay beds. These layers have variable thickness and generally act as good aquifers. Coarse and fine sediment beds alternate, with the coarse layers being most dominant. The presence of gravels in boreholes and facies observed suggests that there are braided paleo-stream channels present which, if developed, can serve as good sources of water supply. The bedrock is fractured, faulted and dips down toward the center of the study area. A prominent bulge in the bedrock is observed in the south of the area and is possibly due to tectonic activity related to the Himalayan orogeny.

In performing the variogram analysis for this data, a spherical model was used which has proved to be a good choice for the 3D mapping of sparse, equally spaced vertical electrical sounding data. In situations where the available data has sufficient coverage and sampling, these techniques can produce valuable geological models for fresh water studies. It should be noted that resistivity techniques possess a set of limitation for stratigraphic and depositional setting studies in saline groundwater systems. The work can be extrapolated

into a basin-wide study for geomorphic and depositional features highlighting the favorable zones for water exploitation with high-resolution resistivity data.

Acknowledgments We would like to acknowledge Dr. Mohammed Soufiane Jouini (Assistant Professor at the Petroleum Institute, Abu Dhabi) for reviewing the statistical aspects of this paper. Water and Power Development Authority (WAPDA) is hereby acknowledged for their support in the present study.

References

- Akhter G, Farid A, Ahmed Z (2012) Determining the depositional pattern by resistivity-seismic inversion for the aquifer system of Maira Area, Pakistan. *Environ Monit Assess* 184(1):161–170
- Armstrong M (1984) Improving the estimation and modeling of the variogram. In: Verly G (ed) *Geostatistics for natural resources characterization*. Reidel, Dordrecht, Holland, pp 1–20
- Balti H, Hachani F, Gamsi M (2013) Hydrogeological potentiality assessment of Teboursouk Basin, Northwest Tunisia using electrical resistivity sounding and well logging data. *Arab J Geosci* 7(7):2905–2914
- Bloemendaal S, Sadiq M (1985) Technical report on groundwater resources in Maira Area, Mardan district, N. W. F. P, WAPDA Hydrogeology Directorate, Peshawar, Report No. IX-1: 40
- Bowling CJ, Rodriguez BA, Harry DL, Zheng C (2005) Delineating alluvial aquifer heterogeneity using resistivity and GPR data. *Ground Water* 43(6):890–903
- Bowling CJ, Harry DL, Rodriguez BA, Zheng C (2007) Integrated geophysical and geological investigation of heterogeneous fluvial aquifer in Columbus Mississippi. *J Appl Geophys* 62(1):58–73
- Bundschuh J (1992) Hydrochemical and hydrogeological studies of groundwater in Peshawar Valley, Pakistan. *Geol Bull Univ Peshawar* 25:23–37
- Burbank DW, Tahirkheli RAK (1985) The magnetostratigraphy, fission-track dating, and stratigraphic evolution of the Peshawar intermontane basin, northern Pakistan. *Bull Geol Soc Am* 96(4):539–552
- Cressie N (1993) *Statistics for spatial data*. Wiley, New York **928**
- Edmund A (2009) Hydrogeological deductions from geoelectric survey in Uvwiamuge and Ekakpamre communities, Delta State, Nigeria. *Int J Phys Sci* 4(9):477–485
- Farid A, Jadoon K, Akhter G, Iqbal MA (2013) Hydrostratigraphy and hydrogeology of the western part of Maira area, Khyber Pakhtunkhwa: a case study by using electrical resistivity. *Environ Monit Assess* 185(3):2407–2422
- Fehdi C, Baali F, Boubaya D, Rouabhia A (2011) Detection of sinkholes using 2D electrical resistivity imaging in Cheria Basin (north-east of Algeria). 4(1–2):181–187
- Geosoft Oasis Montaj (2013) Software for earth science mapping and processing. Geosoft Incorporation Ltd
- Goovaerts P (1997) *Geostatistics for natural resources evaluation*. Oxford University Press Inc, New York **483**
- Gringarten E, Deutsch CV (2001) Teacher's aide: variogram Interpretation and modeling. *Math Geol* 33(4):507–534
- IPI2WIN-1D computer programme (2000) Programs set for 1-D VES data interpretation. Department of Geophysics, Geological Faculty, Moscow University, Moscow
- Kazmi AH, Jan MQ (1997) *Geology and tectonics of Pakistan*. Graphic Publishers, 5C-6/10, Nazimabad, Karachi, p 554
- Kelly WE (1977) Geoelectric sounding for estimating aquifer hydraulic conductivity. *Ground Water* 15(6):420–425
- Kelly WE, Frohlich RK (1985) Relations between aquifer electrical and hydraulic properties. *Ground Water* 23(2):182–189
- Khalil MA, Santos FAM (2013) Hydraulic conductivity estimation from resistivity logs: a case study in Nubian sandstone aquifer. *Arab J Geosci* 6:205–212
- Khan MA, Qureshi RA (1990) Electrical resistivity survey in Naranji area, Swabi and Swat districts, N. W. F. P, Geophysics section, Hydrogeology Directorate, WAPDA, Peshawar, Report No. X-2:15
- Kruseman GP, Naqavi SAH (1988) *Hydrogeology and groundwater resources of the NorthWest Frontier Province, Pakistan*. WAPDA Hydrogeology Directorate, Peshawar, 191 p
- Mazac O, Cislserova M, Vogel T (1988) Application of geophysical methods in describing spatial variability of saturated hydraulic conductivity in the zone of aeration. *J Hydrol* 103(1–2):117–126
- Mhamdi A, Dhahri F, Gousamia M, Inoubli N, Soussi M, Ben Dhia H (2013) Groundwater investigation in the southern part of Gabes using resistivity sounding, southern Tunisia. *Arab J Geosci* 6(2):601–614

- Nizami MMI (1973) Reconnaissance soil survey of Peshawar vale (revised). Soil Survey of Pakistan, Lahore **165**
- Olea RA (1995) Fundamentals of semivariogram estimation, modeling and usage, stochastic modeling and usage. In: Yarus JM, Chambers RL (eds) Stochastic modeling and geostatistics: principles, methods and case studies, 3rd edn. AAPG Computer Applications in Geology, Spain, pp 27–36
- Pogue K, Hussain A (1986) New light on the stratigraphy of Nowshera area and the discovery of Early to Middle Ordovician fossils in N.W.F.P, Pakistan. Geological Survey of Pakistan Information Release no. 135, p 15
- Rafiq M, Jan MQ (1989) Geochemistry and petrogenesis of the Ambela granite complex, NW Pakistan. Geol Bull Peshawar Univ 22:159–179
- Riddell ES, Lorentz SA, Kotze DC (2010) A geophysical analysis of hydro-geomorphic controls within a headwater wetland in a granitic landscape, through ERI and IP. Hydrol Earth Syst Sci 14:1697–1713
- Searle MP, Khan MA, Jan MQ, DiPietro JA, Pogue KR, Pivnik DA, Sercombe WJ, Izatt CN, Blisniuk PM, Treloar PJ, Gaetani M, Zanchi A (1996) Geological map of north Pakistan and adjacent areas of northern Ladakh and western Tibet (Western Himalaya, Salt Ranges, Kohistan, Karakoram and Hindu Kush), prepared from map sheets G-6B, G-6C, G-7A, G-7D, Scale: 1:650,000. Oxford University, UK
- Shah MT, Ali L, Khattak SA (2007) Gold anomaly in the quaternary sediments of Peshawar basin, Shaidu area, district Nowshera, NWFP, Pakistan. J Chem Soc Pakistan 29(2):116–120
- Stauffer KW (1968) Silurian-devonian reef complex near Nowshera, west Pakistan. Bull Geol Soc Am 79(10):1131–1350
- Stewart M, Layton M, Theodore L (1983) Application of resistivity surveys to regional hydrogeologic reconnaissance. Ground Water 21(1):42–48
- Sultan SA, Mekhemer HM, Santos FAM, Abd Alla M (2009) Geophysical measurements for subsurface mapping and groundwater exploration at the central part of the Sinai peninsula, Egypt. Arab J Sci Eng 34(1A):103–119
- Zakir SN, Ihsanullah I, Shah TM, Iqbal Z, Ahmad A (2009) Comparison of heavy and trace metals levels in soil of Peshawar basin at different time intervals. J Chem Soc Pakistan 31(2):246–256
- Zananiri I, Memou T, Lachanas G (2006) Vertical electrical sounding (VES) survey at the central part of Kos island, Aegean, Greece. Geosciences 411–413